Check for updates

Chemistry–A European Journal
Research Article
doi.org/10.1002/chem.202401926
Chemistry Europe
European Chemical Societies Publishing
www.chemeurj.org

Improving Environmental Stress Cracking Resistance of High-Density Polyethylene Grades by Comonomer Addition and Nanocomposite Approach

AmirMohammad Mansouri,[a] Nona Ghasemi Hamedani,[b] Chen Zou,[c] Saber Mousavi,[d] Hossein Ali Khonakdar,[e] Naeimeh Bahri-Laleh,*[e, f] Montserrat Rodríguez-Pizarro,[g] Artur Brotons-Rufes,[g] Sergio Posada-Pérez,*[g] and Albert Poater*[g]

The aim of this paper is to determine the effect of polymer density, correlated to the comonomer content, and nanosilica addition on the mechanical and Environmental Stress Cracking Resistance (ESCR) characteristics of high-density polyethylene (HDPE). In this regard, five HDPE samples with similar Melt Flow Index (MFI) and molar mass but various densities were acquired from a petrochemical plant. Two polymerization reactors work in series and differ only in the amount of 1-buene comonomer fed to the second reactor. To ascertain the microstructure of the studied samples, GPC and SSA (successive self-nucleation and annealing) analyses were accomplished. All samples resulted having similar characteristics but slightly various SCB/1000 C = 7.26–9.74 (SCB=Short Chain Branching). Consequently, meanwhile studied HDPEs reveal similar notched impact and stress at yield values, the tensile modulus, stress-at-break, and elongation-at-break tend to demonstrate different results with the SCB content. More significantly, ESCR characteristic varied considerably with SCB/1000 C extent, so that higher amount of SCB acknowledged advanced ESCR. Notably, blending HDPE sample containing higher amount of SCB/1000 C, with 3 wt.% of chemically modified nanosilica enhanced ESCR characteristic by 40 %. DFT (Density Functional Theory) calculations unveiled the role of the comonomer, quantitatively by binding energies and qualitatively by Non Covalent Interaction (NCI) plots.

Introduction

Polyethylene (PE) is the most important family of thermoplastics resins in the world.[1] According to density, this polymer is classified into low density PE (LDPE), linear low-density PE (LLDPE) and high density polyethylene (HDPE). Among them, the latter two are formed via coordination polymerization of ethylene feedstock by transition metal catalysts, especially Ziegler-Natta type.[2] HDPE is a semi-crystalline polymer containing almost ethylene-based linear chains with a small content of 1-butene or 1-hexene comonomer, to force short chain branching (SCB) into the fully extended linear polymeric chain.[3] This polymer is the most widely used plastic, it has been able to find a wide range of applications, including storage containers for chemicals, foods or liquids, as well as toys, pipes, geocellular networks, and plastic films,[4] and can also be combined with nanostructures.[5]

Despite its appreciable characteristic, HDPE is susceptible to a phenomenon known as Environmental Stress Cracking (ESC), when the polymer is used as pipes, geocellular networks and geomembranes.[6] This failure happens because of the ductile nature of HDPE and occurs when the material is subjected to a constant tensile stress that is lower than its yield stress.[7] Indeed, due to the crystalline nature of HDPE, at high tensile stresses, this material will stretch and yield prior to failure.[8] However, when HDPE is continuously exposed to a low tensile stress in an active environment, it fails abruptly with a smooth rupture, which is related to its brittle failure and ESC. In fact, active environment (for example solutions containing surfactants favors the disentanglements of tie molecules in proximity of a defect/notch/crack If the latter is not present only slow crack growth will occur.[9] The accepted mechanism for HDPE failure in active environment is that the active solution can diffuse within the crazes leading to the material plasticization.

[a] A. Mansouri
Kermanshah Polymer Petrochemical Company, Kermanshah, Iran
[b] N. Ghasemi Hamedani
National Petrochemical Company-Research and Technology Co.(NPC-RT), Tehran, Iran
[c] C. Zou
Department of Polymer Science and Engineering, University of Science and Technology of China,Hefei 230026, China
[d] S. Mousavi
Lorestan Petrochemical Company, Lorestan, Iran
[e] H. A. Khonakdar, N. Bahri-Laleh
Iran Polymer and Petrochemical Institute (IPPI) P.O. Box 14965/115 Tehran, Iran
E-mail: n.bahri@ippi.ac.ir
[f] N. Bahri-Laleh
Institute for Sustainability with Knotted Chiral Meta Matter (WPI-SKCM2), Hiroshima University, Hiroshima 739-8526, Japan
[g] M. Rodríguez-Pizarro, A. Brotons-Rufes, S. Posada-Pérez, A. Poater
Institut de Química Computacional i Catàlisi, Departament de Química, Universitat de Girona,c/ Mª Aurèlia Capmany 69, 17003 Girona, Catalonia, Spain
E-mail: albert.poater@udg.edu
sergio.posada@udg.edu

Supporting information for this article is available on the WWW under https://doi.org/10.1002/chem.202401926

© 2024 The Author(s). Chemistry - A European Journal published by Wiley-VCH GmbH. This is an open access article under the terms of the Creative Commons Attribution License, which permits use, distribution and reproduction in any medium, provided the original work is properly cited.

© 2024 The Author(s). Chemistry - A European Journal published by Wiley-VCH GmbH

Therefore, interaction forces between the polymeric macromolecules reduce which eventually favors their mutual disentanglement.[10] It is important to note that the brittle or ductile behavior of HDPE depends on the temperature and loading conditions such as strain rate, constant stress level or others depending on the applied mechanical history.[11,12] To use HDPE in these environments, its resistance to ESC must be enhanced.[13] This especial HDPE is regarded as a high Environmental Stress Cracking Resistance (ESCR) HDPE grade.[14]

Chain branching, whether short or long chain branching, is the most important parameter affecting the ESC feature. It is true that molecular weight and branching are the main structural parameters affecting polymer ESCR. However, according to the literature, the significance of side chain branches is higher compared to molecular weight.[15] In fact, ESC does not occur (or occurs in harsher environments and higher stresses compared to HDPE) in medium density PE and LLDPE containing higher SCB contents. However, in some applications such as pipes and membranes, high crystallinity, that is correlated to excellent mechanical characteristics, is required, originating from a higher density of HDPE.[16,17] Therefore, the simplest solution is to regulate and tailor the SCB content and distribution in HDPE in order to avoid ESC.[18]

It is worth mentioning that more than 70% of HDPEs are commercially produced using Ziegler-Natta catalysts.[19,20] These catalysts are almost based on $TiCl_4/MgCl_2$ precursors and can produce a wide range of PEs with densities in the range of 0.939 to 0.960 g/cm^3.[21] Despite their commercial importance, as well as regardless of the outstanding advances in the production of industrially relevant catalysts with good spherical morphology and easy operation conditions in industrial polymerization reactors,[22,23] these catalysts suffer from a low comonomer affinity and the lack of long chain branching.[24,25] Consequently, achieving low density through the Ziegler-Natta process is ambitious, because of the wide range of applications.[26]

From the early years of commercial development of polyethylene, ESCR has played a major role in defining the end use applications and expanding the market for HDPE resins. It is well accepted that by adjusting the density of commercial HDPE to its lowest grade, the ESC can be greatly improved. In fact, there should be an indirect relationship between polymer density and ESC strength. However, this relationship has not been quantified so far. In the current research, five HDPE injection molding grades with different densities have been assessed by different analytical tools to quantify the relationship between polymer density and ESC resistance characteristic, together with predictive Density Functional Theory (DFT) calculations.[27,28]

Results and Discussion

Catalyst Characterization

As mentioned in the Experimental section, an industrial heterogeneous $MgCl_2$ (ethoxide type)/$TiCl_4$ Ziegler-Natta catalyst is employed in an industrial polymerization plant with 300 kt/y capacity to furnish HDPE samples. The components, particle size and size distribution, surface area and pore characteristic of the catalyst are listed in Table 1.

Notably, the catalyst has a Ti content of 5.5%, surface area of 129 m^2/g, average pore diameter of 11.2 nm, X50 of 9.4 μm and SPAN of 1.7, which are acceptable values for the slurry phase ethylene polymerization catalysts.[29]

Then, the morphology of the catalyst was observed by SEM analysis. In the related pictures included in Figure 1, an outstandingly uniform spherical morphology of catalyst particles is appreciated. This unique morphology is required in industrial plants, to facilitate powder and slurry conveying among different units (between reactors, and from the second reactor to the centrifuge, dryer and extruder).[2,30] Moreover, in the EDX analysis the presence of Ti, Mg, Cl and C elements is confirmed. Ti and Cl are representative of $TiCl_4$ precursor, while Mg and Cl are correlated to the $MgCl_2$ support. The C content is attributed either to the donor or remained ethoxide moiety of the primary magnesium ethoxide precursor. According to the elemental maps, an almost uniform distribution of mentioned elements is adopted which leads to a similar polymerization rate in the growing polymer chains. Non-uniform spread of active centers has been reported to cause non-homogenous distribution of stress in polymer particles and their rupture.[31]

To fulfill the requirements of an efficient Ziegler-Natta catalyst for the olefin polymerization process, the magnesium ethoxide should possess appropriate locations for the absorption of the active Ti precursor, in order to minimize its leaching during the polymerization experiment and produce HDPEs with a tailored microstructure. It is well established that $TiCl_4$ preferentially adsorbs on specific lateral cuts of the $MgCl_2$ surface, such as (110), (104) and (100). In other words, strong adsorption occurs exclusively on these surfaces.[32] During support preparation steps, its crystalline structure changes considerably.[33,34] To confirm this issue, an XRD analysis of pristine $Mg(OEt)_2$ and final catalyst was carried out. Figure S1 clearly confirms that the diffraction pattern of catalyst differs dramatically from that of the primary $Mg(OEt)_2$ originated from the change of support crystalline texture during its modification and catalyst synthesis processes. Unreacted $Mg(OEt)_2$ displays sharp peaks centered at 2θ of 9.5, 11.9, and 23.2, associated with its crystalline structure. In the catalyst, these peaks

Table 1. General characteristics of employed Ziegler-Natta catalyst in industrial reactors.

	Ti:Mg:Cla	Ti (wt.%)	Surface area (m^2/g)	Total pore volume (cm^3/g)	Average pore diameter (nm)	X10 (μm)	X50 (μm)	X90 (μm)	SPAN[b]
Amount	0.3:1.0:2.9:	5.5	129	0.890	11.2	4.3	9.4	20.6	1.7

[a] In weight percentage, [b] SPAN = (X90–X10)/X50

© 2024 The Author(s). Chemistry - A European Journal published by Wiley-VCH GmbH

15213765, 2024, 54, Downloaded from https://chemistry-europe.onlinelibrary.wiley.com/doi/10.1002/chem.202401926 by Universitat de Girona, Wiley Online Library on [09/12/2024]. See the Terms and Conditions (https://onlinelibrary.wiley.com/terms-and-conditions) on Wiley Online Library for rules of use; OA articles are governed by the applicable Creative Commons License

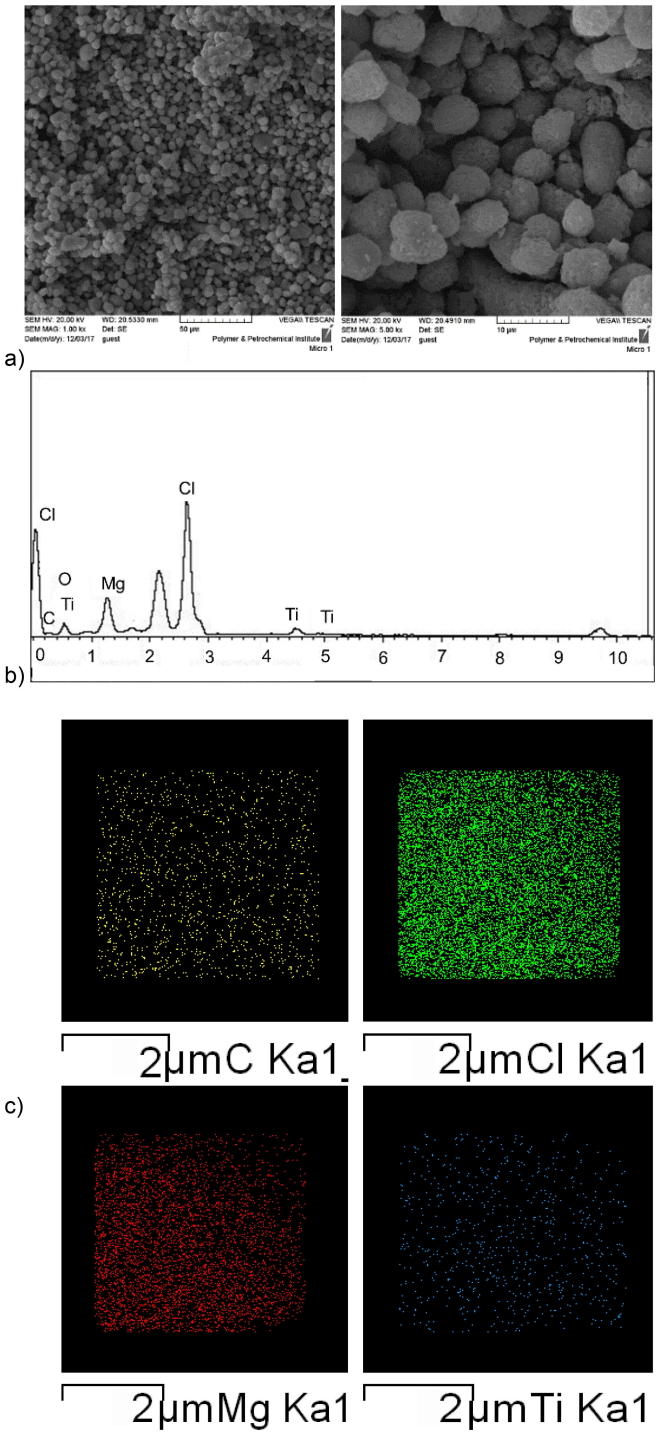

Figure 1. (a) SEM pictures, (b) EDX analysis and (c) elemental maps of the commercial catalyst employed in the production of studied HDPE grades.

disappeared and were replaced with new ones at $2\theta = 17$, 23, 28, 32, 43, 45 and 62°, attributed to the structurally disordered δ-$MgCl_2$.[35] This outcome confirmed well the conversion of $Mg(OEt)_2$ to $MgCl_2$ during catalyst synthesis.[36] Indeed, in this step a Cl-OEt exchange occurs between magnesium ethoxide and Cl-donor species (such as $TiCl_4$ and/or organic halides) which furnishes final $MgCl_2$.

HDPEs Microstructures

The catalyst was employed in the production of five HDPE samples, in a plant with 300 kt/h capacity, with different 1-butene content in the feed. The attributed reaction conditions to synthesize the targeted samples are included in Table 2. It is worth mentioning that ethylene, catalyst, cocatalyst and hydrogen (as a chain transfer agent) are fed into the first reactor,[37] while ethylene and 1-butene are charged to the second reactor. However, a very small amount of hydrogen is observed in the second reactor, correlated to soluble H_2 in the recycled hexane which is fed into the reactor as the slurry media. In fact, hexane as a slurry medium is separated from the polymer powder after the second polymerization reactor and in the drying section, which after recycling in the distillation towers is re-used in the plant. This recycled hexane contains small amounts of soluble ethylene, hydrogen, co-catalyst and 1-butene comonomer. Recycled hexane is fed to both reactors, and depending on the amount of impurities, it can somehow alter the characteristics of the polymer obtained in each reactor. This configuration of starting materials, *i.e.* a very large amount of H_2 in the 1st reactor, a lower temperature of the 1st reactor, and the feed of the 1-butene comonomer to the 2nd reactor, ensures the desired bimodality and the insertion of short chain branching at high molar mass PE chains, which are advantages for polymer processing.

Density and MFI are the most important characteristics that are controlled carefully in any industrial HDPE plant. The MFI data of the studied samples collected at two weights of 5.0 and 21.6 kg, as well as their ratios, FRR, are included in Table 3. It is worth mentioning that since the GPC analysis is costly and time consuming, in the industrial polyolefin plants the polymer molar mass and flow-ability are traced by MFI and FRR experiments. In fact, the mentioned characteristics are directly correlated to the polymer molar mass and dispersity (Đ). Among the samples, HDPE-3 followed by HDPE-2 has slightly lower MFIs, but the difference is not noticeable.

The molar mass and its distribution of commercial HDPEs play an important role in the polymer classification in industry. According to the reported data in Table 3 it can be deduced that the samples have similar characteristics with M_n and $Đ = M_w/M_n$ of about 51,000–54,000 g/mol and 7.2–7.8, respectively. Indeed, this outcome is expected since R1 and R2 reactors were operated in similar reaction conditions to produce studied samples. This deduction was further confirmed by the deconvolution of the experimentally obtained GPC curves into a weighted summation of appropriate Gaussian distribution functions (Figure S2b–e). Using this procedure, the number and productivity of each active center in heterogeneous catalysts is also quantified. Notably, the samples have a similar non-uniformity in chain lengths, arising from six different active sites in the employed Ziegler-Natta catalyst. In the studied HDPE samples, the molar mass of the first two Flory peaks (active sites I and II) are lower than 7000 g/mol and these components constitute approximately 20% of the total peaks (Table S1). The related catalytic sites are almost active in the 1st reactor in which a large amount of H_2 is fed and are responsible for the

© 2024 The Author(s). Chemistry - A European Journal published by Wiley-VCH GmbH

15213765, 2024, 54, Downloaded from https://chemistry-europe.onlinelibrary.wiley.com/doi/10.1002/chem.202401926 by Universitat de Girona, Wiley Online Library on [09/12/2024]. See the Terms and Conditions (https://onlinelibrary.wiley.com/terms-and-conditions) on Wiley Online Library for rules of use; OA articles are governed by the applicable Creative Commons License

15213765, 2024, 54, Downloaded from https://chemistry-europe.onlinelibrary.wiley.com/doi/10.1002/chem.202401926 by Universitat de Girona, Wiley Online Library on [09/12/2024]. See the Terms and Conditions (https://onlinelibrary.wiley.com/terms-and-conditions) on Wiley Online Library for rules of use; OA articles are governed by the applicable Creative Commons License

Table 2. Operation conditions of two reactors (R1 and R2) and MFI of produced HDPEs. Plant production capacity is 40 t/h.

R2					R1				
MFI_5	1-Butene (kg/h)	H2/C2[a]	P (bar)	T (°C)	MFI_5	H2/C2[a]	P (bar)	T (°C)	HDPE label
1.3	272	0.11	4.0	81	557	3.1	8.9	84	HDPE-1
1.2	239	0.10	4.0	81	540	3.1	9.1	84	HDPE-2
1.2	210	0.11	4.2	81	538	3.1	9.1	84	HDPE-3
1.3	169	0.12	4.5	82	558	3.1	8.8	84	HDPE-4
1.2	139	0.11	4.3	82	542	3.0	9.2	84	HDPE-5

[a] Weight ratio of hydrogen to ethylene in the feed.

Table 3. Molar mass and MFI characteristics of studied HDPE samples.

HDPE label	Density (g/cm^3)	MFI_5 (g/10 min)	$MFI_{21.6}$ (g/10 min)	FRR[a]	Mn (g/mol)	Đ[b]
HDPE-1	0.952	0.95	18.59	18.98	53400	7.36
HDPE-2	0.953	0.90	18.34	20.44	51400	7.57
HDPE-3	0.953	0.89	18.03	21.29	51100	7.79
HDPE-4	0.954	0.97	18.95	18.91	52500	7.25
HDPE-5	0.955	0.92	18.40	20.21	51600	7.48

[a] FRR=$MFI_{21.6}/MFI_5$., [b] $Đ = M_w/M_n$.

good processability of the final polymer. On the other hand, the molar mass of polymer chains formed via active centers V and VI comprise approximately 30% of the total chains. The so-called fractions have high molar masses with $M_n > 260{,}000$ g/mol and are responsible for the improvement of the mechanical properties. All samples enjoy both high and low molar mass chains, thanks to the multi-site nature of Ziegler-Natta catalysts and advanced two reactors technology, to ensure good mechanical properties and high processing capacity.

Successive self-nucleation and annealing (SSA) was applied to thermally fractionate the polymeric samples. The final SSA endotherms were deconvoluted into the weighted sum of seven peaks, using Peakfit 4.12 software and the standard Gaussian distribution function. The results are illustrated in Figure S3. Each peak in the endothermic melting curves is assumed to correspond to a crystalline fraction of samples with a similar thickness. The quantitative evaluation of each melting peak was calculated using the Gibbs – Thomson equation and related equations (See supporting information file).[70] The average lamellar thickness ($\overline{L}$),[38–40] average branches per 1000 carbon atoms ($\overline{SCB}$) and average comonomer content distribution ($\overline{CCD}$) were calculated and listed in Table 4. The corresponding discrete distribution of melting endotherms, lamellar thickness and SCB are illustrated in Figure 2, as well. The difference between these industrial samples is clearly depicted in the SSA results. As the density increases from HDPE-1 to HDPE-5, the population of chains that melt at higher temperatures increases.[41] It is also clear that with increasing comonomer content, lamellar thickness is placed in a more limited range and the distribution of short chain branches becomes more uniform. It could lead to the increase of homogeneity of chains which improves the properties of the final product.[70] It should be noticed that the molar mass of studied samples is at the same level, therefore, the difference in the sample properties is expected to arise through various degrees of comonomer incorporation.[42] In fact, molar mass and comonomer incorporation play a major role in tailoring an HDPE microstructure,[43] when one variable (molar mass) is kept constant, the effect of the second parameter can be deeply and accurately understood, which is the main aim of the present investigation.

Table 4. Different characteristics of the studied samples obtained from SSA and DSC analyses.

HDPE label	$\overline{L}$ (nm)[a]	$\overline{SCB}$[b]	$\overline{CCD}$ (mass%)[c]	%C4[d] (Wt.%)	X_c (%)	T_m (°C)
HDPE-1	14.37	9.74	3.89	3.5	56.57	138.78
HDPE-2	14.32	8.29	3.31	3.0	56.85	137.96
HDPE-3	15.14	8.04	3.21	2.8	62.45	138.98
HDPE-4	15.90	7.35	2.94	2.7	62.73	137.94
HDPE-5	16.80	7.26	2.90	2.5	66.73	139.35

[a] Crystal thickness. [b] Branches per thousand carbon atoms. [c] The percentage of C4 comonomer. [d] Comonomer content determined by FTIR.

© 2024 The Author(s). Chemistry - A European Journal published by Wiley-VCH GmbH

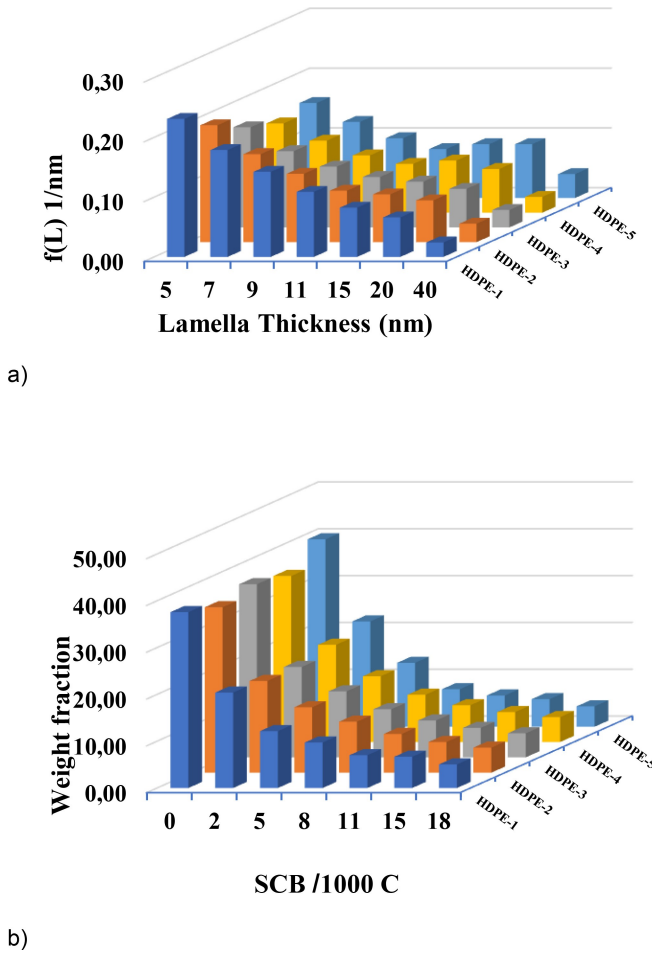

Figure 2. (a) Discrete distributions of lamellar thickness, and (b) SCB/1000 C of studied HDPEs.

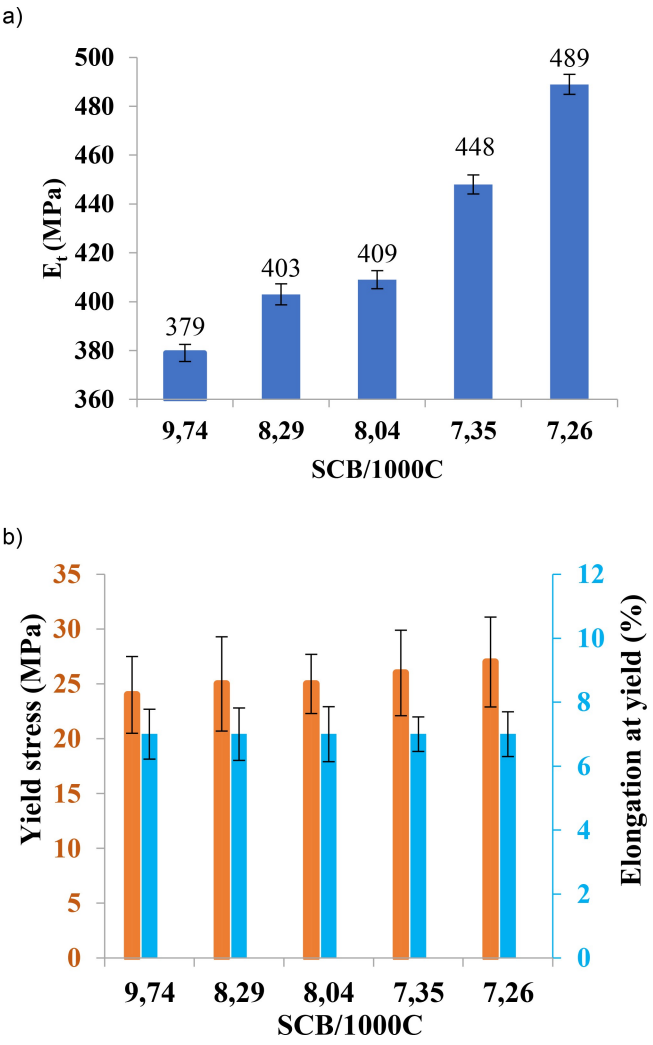

Figure 3. (a) Young's modulus (E_t), (b) yield stress and elongation at yield of the studied HDPE samples obtained from stress-strain curves.

Mechanical Properties

Tensile and notched impact are among the principal tests to characterize the mechanical properties of polymers. The tensile curves are demonstrated in Figure S4. Several important parameters are derived from these curves, including tensile modulus (E_t); yield stress (σ_Y); elongation at yield (ε_Y); stress at break (σ_B); and elongation at break (ε_B). The derived data are collected in Table 5. Also, Figure 3 demonstrates variation of the modulus, yield stress and elongation at yield with the comonomer content for the studied HDPE samples. It can be clearly seen that E_t, σ_B and ε_B depend considerably on the comonomer content. The higher the SCB/1000 C, the greater the σ_B and ε_B and the lower the E_t.[44] This deduction would be connected to the lamellar thickness (L) of the polymers (Table 5). In the HDPE-1 and HDPE-2 samples that include thinner lamellars, the number/length of tie molecules increases that can extend after yield stress and form new crystal domains. These newly formed domains enhance σ_B, considerably.[45,46] In

Table 5. Mechanical properties of studied HDPE samples.

	E_t (Mpa)	σ_Y (MPa)	ε_Y (%)	σ_B (MPa)	ε_B (%)	Notched Impact (kJ/m^2)
HDPE-1	379	24	7	38	738	14.0
HDPE-2	403	25	7	34	678	13.7
HDPE-3	409	25	7	29	674	14.5
HDPE-4	448	26	7	28	656	13.9
HDPE-5	489	27	7	22	598	13.5

E_t: Tensile modulus; σ_Y: Stress at yield; ε_Y: Elongation at yield; σ_B: Stress at break; ε_B: Elongation at break 1 > 2 > 3 > 4 > 5.

© 2024 The Author(s). Chemistry - A European Journal published by Wiley-VCH GmbH

15213765, 2024, 54, Downloaded from https://chemistry-europe.onlinelibrary.wiley.com/doi/10.1002/chem.202401926 by Universitat de Girona, Wiley Online Library on [09/12/2024]. See the Terms and Conditions (https://onlinelibrary.wiley.com/terms-and-conditions) on Wiley Online Library for rules of use; OA articles are governed by the applicable Creative Commons License

fact, in crystalline domain the polymer chains fold and lamellars arrange in a regular manner. In HDPE, containing 1-butene unit as comonomer, the folding happens in the place where comonomer is embedded. So, by increasing comonomer (SCB/1000 C) content, the number of folds increases, leading to the formation of thin lamellars with long tie molecules which eventually enhances σ_B and ε_B.

Notched impact was also measured to see the resistance of HDPEs to sudden force. As a remark, no considerable changes were found in the notched impact characteristic compared to polymer density or SCB/1000 C values (Table 5).

Finally, the ESCR test was carried out at T = 50 °C on the HDPE samples and their failure times against polymer density and SCB/1000 C are collected. This test was repeated three times for each sample, and the average values are reported here with an accuracy of ±4%, in agreement with past applications.[47] According to Figures 4a and b, there is a distinct difference among ESCR values and increases with decreasing polymer density or increasing short chain branching content. It is worth mentioning that ESCR improves with both polymer molar mass and SCB content characteristics. Since the studied HDPE samples have similar molar mass and MFI, see Table 3, the ESCR improvement is directly correlated to the SCB content. According to the literature, with increasing SCB content, craze initiation and crack growth is prevented. Indeed, in the ethylene/α-olefin copolymers the long sequence of ethylene units is predicted to constitute crystallizable sections, whereas SCB or α-olefin are responsible for the non crystallizable sequences. Therefore, increasing the SCB content to a limit facilitates the formation of tie molecules. In polymer chains with similar molar mass, the tie molecule length increases by increasing the SCB level, which is a key factor in ESCR improvement. It is worth mentioning that, beside the SCB content, the distribution of α-olefin monomer within polymer chain is a determining factor that influences the ESCR characteristic.[48] However, since the samples are produced via the same catalyst, they exhibit a similar α-olefin distribution trend, see SSA curves in Figure S3, which rules out the effect of this important parameter.

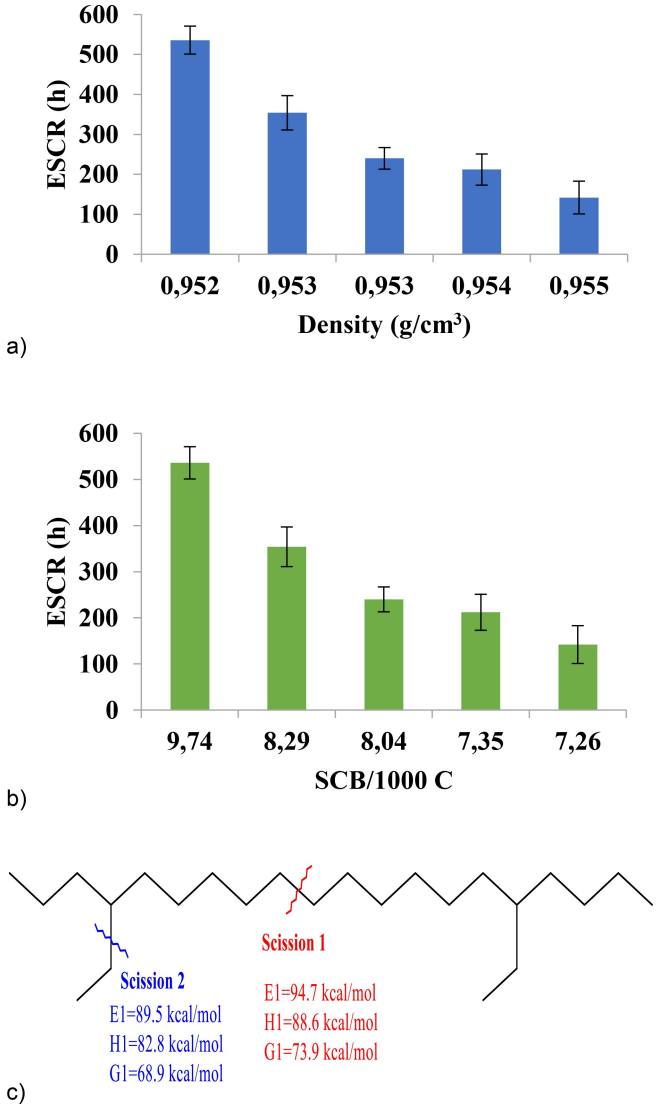

Figure 4. Effect of HDPEs: (a) density and (b) SCB on ESCR results and (c) scheme of studied chain scissions.

According to the ESC results, HDPE-1 with the lowest density of 0.952 g/mL reveals the longest failure time of 536 h. This is further confirmed in Figure 4b, which demonstrates the effect of SCB/1000 C on the ESCR strength. Accordingly, at densities greater than 0.953 g/mL, or SCB/1000 C lower than 8.29, the improvement in ESCR strength is not appreciable. However, at slightly higher SCB contents, 8.29 ≥ SCB/1000 C, ESCR improves considerably.

Origin of ESCR

In this section, the origin of ESCR is described in brief, experimentally and computationally. Generally, polymer failure is occurred as the consequence of two different phenomena: i) bond scission, which is directly attributed to the molecular strength and ii) the displacement of polymer chains and coils in/between amorphous, crystalline and interface regions. The latter is referred to "chain or tie molecule disentanglement". In order to shed light on the true origin of ESCR and avoid misunderstanding about chain scission and ESC concepts, the dissociation energy needed to homolytically cleave a CH_2–CH_2 bond (representative of un-branched HDPE moiety), and CH_2CH–CH_2 bond (representative of SCB, or comonomer presence) was calculated by molecular simulation of a model HDPE chain, containing 8 ethylene and two 1-butene monomer units (Figure 4c). In the mentioned calculations, a $\triangle G_1 = 73.9$ and $\triangle G_2 = 68.9$ kcal/mol were obtained, confirming the easier dissociation/degradation of polymer chain possessing butene co-monomer. This is correlated to the higher stability of secondary C• radicals, formed via Scission 2 mechanism, in comparison with the stability of first C• radical formed via Scission 1 mechanism (Figure 4c). Consequently, SCB facilitates chain scission, while improving ESCR property. In fact, the mechanisms deal with in the ESC phenomenon and chain scission are different and should not be confused.

© 2024 The Author(s). Chemistry - A European Journal published by Wiley-VCH GmbH

15213765, 2024, 54, Downloaded from https://chemistry-europe.onlinelibrary.wiley.com/doi/10.1002/chem.202401926 by Universitat de Girona, Wiley Online Library on [09/12/2024]. See the Terms and Conditions (https://onlinelibrary.wiley.com/terms-and-conditions) on Wiley Online Library for rules of use; OA articles are governed by the applicable Creative Commons License

Indeed, resistance toward ESC is correlated to the larger population of tie molecules linking HDPE's crystalline regions, by enhancing the SCB content.[49] In general, domains susceptible to stress crack initiation are less prevalent in polymer domains comprising high SCB content chains.[50] This is the main reason for the ESCR improvement with the enhancement of SCB content. Going to do an analysis of what happens if the chains have or do not have ethyl substituents, there is a disparity of results. Also, without any substituent the formation of the species with 2 units is 9.0 kcal/mol less stable, with 3 units up to 16.1 kcal/mol. But the latter structure can be as much as 0.2 kcal/mol above the single chain, if the 3 chains are arranged in nearly c3v geometry instead of the planar arrangement. And for the latter structure, chain cleavage by a $C(H_2)$–$C(H_2)$ bond was also studied, requiring 73.2 kcal/mol, thus at almost the same cost as chains with substituents ethyl in them. Turning the discussion to the single chain bearing ethyl substituents, going to 2 chains destabilizes by 2.3 kcal/mol, while with 3 it becomes more stable by 1.4 kcal/mol, and it is critical that the 3 chains are together, because if they are placed in the same plane there is a destabilization of 4.6 kcal/mol, therefore this isomer is 6.0 kcal/mol above the other. Repeating the radical decomposition analysis with not 1 but 2 chains, when an ethyl chain dissociates as a radical, the destabilization is 66.4 kcal/mol, while 76.5 kcal/mol when breaking a $C(H_2)$–$C(H_2)$ bond. Therefore, there is a decrease of 2.5 kcal/mol in the first case, and an increase of 2.6 kcal/mol in the second. Thus, when chains are added, the dissociation of the ethyl becomes even easier while the breaking of a chain, in accordance with the above-mentioned reasoning from the experiments.

It is intriguing the possible interactions between chains, with a typology of intrinsic forces between eminently non-polar species.[51,52] In detail, to computationally evaluate the non-covalent interactions that may exist between the polymeric chains, the Non Covalent Interaction (NCI) plots[53,54] of Contreras and coworkers were used. In detail, NCI plots are graphical representations used in computational chemistry to visualize the distribution of non-covalent interactions within molecular systems. These interactions, such as hydrogen bonding, van der Waals interactions, π-π stacking, and electrostatic interactions, play crucial roles in determining the structure, stability, and properties of molecules and molecular complexes. The definition of NCI plots involves plotting the electron density of a molecular system and highlighting regions where attractive (blue) and repulsive (red) interactions dominate. In further detail, regions with high RDG values typically indicate the presence of strong noncovalent interactions. The color scale is used to represent the strength and nature of interactions. Typically, the color scale is associated with the sign and magnitude of the second density Hessian eigenvalue. Negative values (in shades of red) indicate repulsive interactions, while positive values (in shades of blue) represent attractive interactions.[51] These plots are typically generated using quantum mechanical calculations, particularly DFT methods, to map out regions of significant interaction strength. Thus, knowing that the 3D NCI plots provide a graphical representation of noncovalent interactions within a molecular system, noncovalent interactions include various forces such as hydrogen bonding,[55] van der Waals interactions, and other weak interactions that play a crucial role in molecular structures, properties, and reactions.[56,57] In detail the 3D plot consists of isocontours, which are surfaces representing regions of constant electron density. These contours help visualize the distribution of electrons within the molecular system. In addition, the isocontours are often based on the reduced density gradient (RDG), a mathematical parameter that characterizes the electron density's variations.

Figure 5a with the three-dimensional arrangement already allows us to make an incipient conclusion that with ethyl substituents there is a greater preponderance of interactions, but where it can be felt, and almost quantitatively, is in Figure 5b which includes the two-dimensional plots,[58,59] using the reduced density gradient (RDG). Bidimensional NCI plots provide a visual representation of noncovalent interactions in a molecular system, but unlike their three-dimensional counterparts, they are projected onto a two-dimensional plane.[58] Thus, the density of the central part indicates a much more than significant increase when ethyl molecules are included, and the effect of arranging the 3 chains in a two-dimensional or three-dimensional way, that is, in a planar way or with a more compact arrangement, respectively. These results confirm the low crystallization of chains with high SCB content that can be the exact origin of the ESCR improvement. It is necessary to hypothesize that perhaps in the future an effort should be made towards dynamic calculations to see what stiffness these weak interactions between chains give. And if a certain order is achieved in carrying out the experiments, periodic calculations can be carried out.[60]

HDPE-1/Modified-silica Nanocomposites

Due to the advanced ESCR characteristics of HDPE-1, this polymer was selected as the optimal HDPE grade and in the following, the effect of nanosilica loading on its ESCR properties was investigated. Due to the extremely polar nature of nanosilica and non-polar characteristic of polyolefins, its incorporation into the polymer matrix is a major challenge.[61] To overcome this drawback, functionalization of nanosilica particles with a copolymer of hexane/hexanol was accomplished. According to the previous study by some of us,[62] fully homogenous polyethylene/silica nanocomposites can be developed using this strategy. With this aim, the first mentioned copolymer was synthesized by a simple cationic route,[63] using the $AlCl_3$ co-initiator. GPC analysis revealed $M_n = 1700$ g/mol and $Đ = 1.4$ for the synthesized copoly(hexane/hexanol), Figure 6a. Also, according to ^{1}H NMR analysis, Figure 6b, the appearance of peaks at 0.91 (CH_3), 1.29 (CH and CH_2), 2.04 (CH allylic), 3.67 (CH_2–OH), 4.0–5.1 (RCH=CHR′), affirms the inclusion of OH functionality in the polyolefin backbone.

The synthesized hexane/hexanol copolymer was then grafted onto the nanosilica surface by a simple etherification reaction between OH groups on the silica surface and the copolymer. To confirm the success of the grafting reaction, FTIR

© 2024 The Author(s). Chemistry - A European Journal published by Wiley-VCH GmbH

15213765, 2024, 54, Downloaded from https://chemistry-europe.onlinelibrary.wiley.com/doi/10.1002/chem.202401926 by Universitat de Girona, Wiley Online Library on [09/12/2024]. See the Terms and Conditions (https://onlinelibrary.wiley.com/terms-and-conditions) on Wiley Online Library for rules of use; OA articles are governed by the applicable Creative Commons License

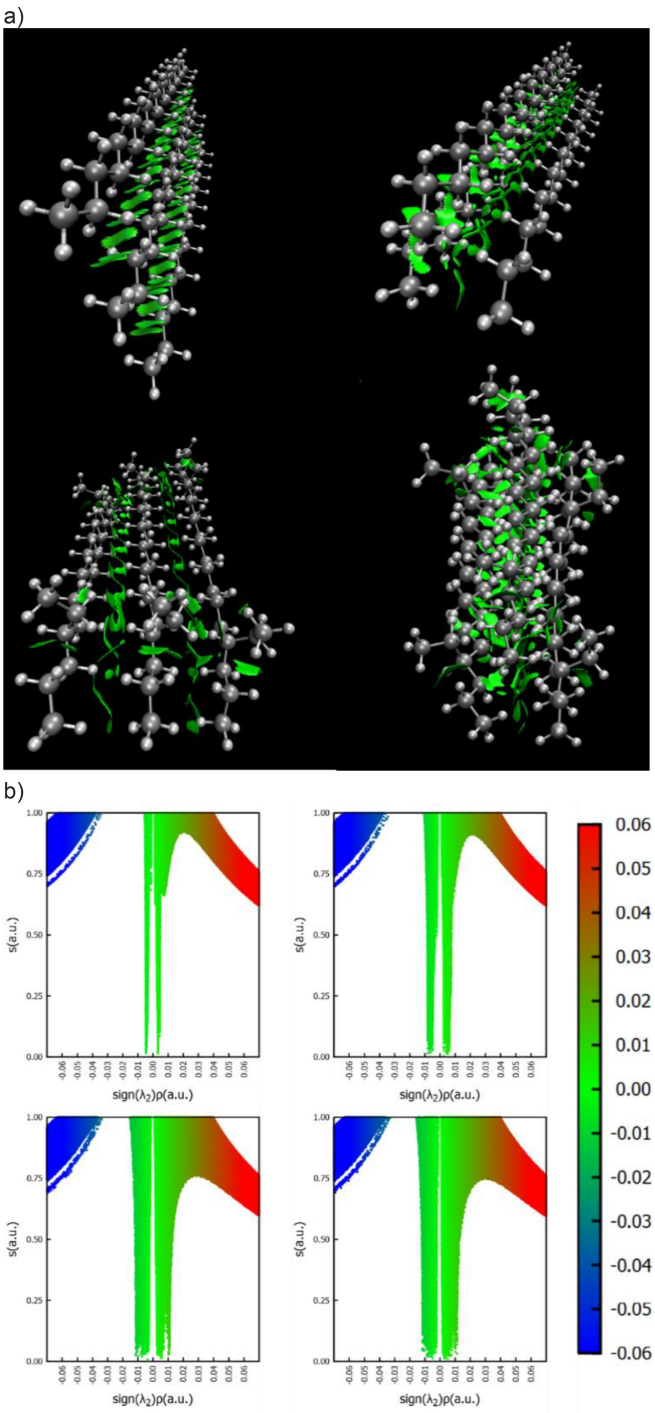

Figure 5. NCI plots with 3 chains: (a) 3D and (b) 2D of the reduced density gradient (S) vs sign(l_2)r, in a.u. for planar (left) and compact (right) conformation of the chains, without (top) or with (below) ethyl substituents.

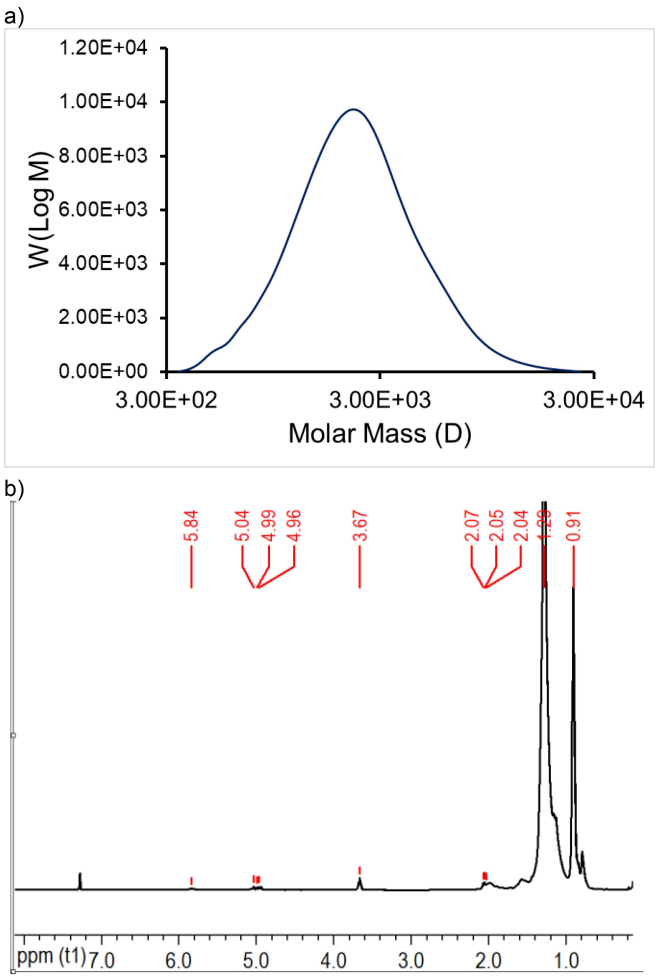

Figure 6. (a) GPC curve and (b) H NMR spectrum of the synthesized copoly(hexane/hexanol).

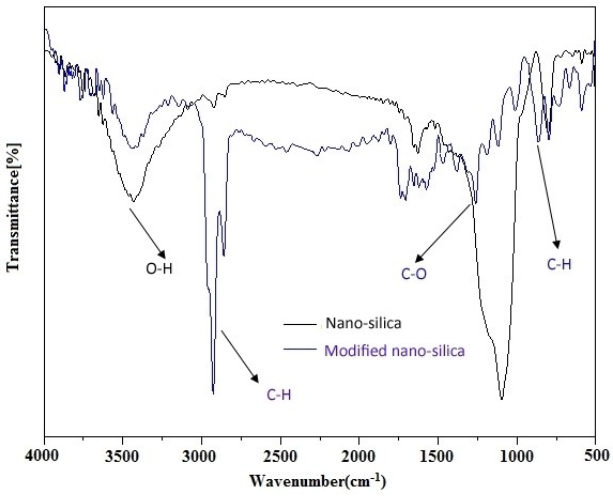

Figure 7. FTIR spectra of primary nanosilica particles and the modified nanosilica with copoly(hexane/hexanol).

spectroscopy was accomplished in Figure 7. According to the spectrum, the product exhibited some distinct peaks at 1225 cm^{-1} (C–O stretching), 2910 cm^{-1} (C–H stretching vibration) and 810 cm^{-1} (C–H rocking), affirmed the successful chemical bonding between the synthesized copolymer and the nanosilica surface.[64]

A blend of HDPE-1, containing a maximum amount of SCB, with 3 wt.% of the modified nanosilica was prepared via melt blending in a 60 mL Brabender type internal mixer (GmbH & Co., Germany) at T = 180 °C, rotor speed = 80 rpm and t = 7 min. To characterize the dispersion quality of the modified silica in

© 2024 The Author(s). Chemistry - A European Journal published by Wiley-VCH GmbH

15213765, 2024, 54, Downloaded from https://chemistry-europe.onlinelibrary.wiley.com/doi/10.1002/chem.202401926 by Universitat de Girona, Wiley Online Library on [09/12/2024]. See the Terms and Conditions (https://onlinelibrary.wiley.com/terms-and-conditions) on Wiley Online Library for rules of use; OA articles are governed by the applicable Creative Commons License

the HDPE-1 matrix, the XRD analysis in Figure 8a was considered.

Neat silica revealed a diffraction peak at 2θ of 23°, which was shifted down to 2θ = 18°, because of the destruction of the layered structure of silica nanoparticles. This is the result of the silica modification strategy leading to a better interaction between HDPE-1 and silica nanoparticles. Notably, the TEM picture in Figure 8b confirmed the XRD result towards a good dispersion of modified nanosilica particles in the HDPE-1 matrix.

In the ESCR test, the prepared nanocomposite revealed a very advanced ESC characteristic of 750 h. Indeed, as the consequence of the strategy employed in modifying the silica hydrophobicity, and its uniform dispersion in the HDPE-1 matrix, the ESCR characteristic was increased up to 40%. The ESCR test was repeated three times for the nanocomposite sample, and the average value is reported here with an accuracy of ±4%.

According to the literature, the crack propagation rate diminishes in the presence of inorganic nanofillers.[65] In fact, in the fracture surface beside plastic deformation, numerous tiny structures and cavities are formed in hyperbolic shape. Nanofillers and their aggregates serve as stress concentrators in plastic matrix, enhancing the formation of the mentioned structure. Furthermore, particle debonding and cavities formation are promoted in the presence of nanofillers, which together with crack deflection of matrix and localized microdeformation cause energy dissipation which eventually improves the fracture toughness of nanocomposites and reinforces the plastic ESCR.[66,67]

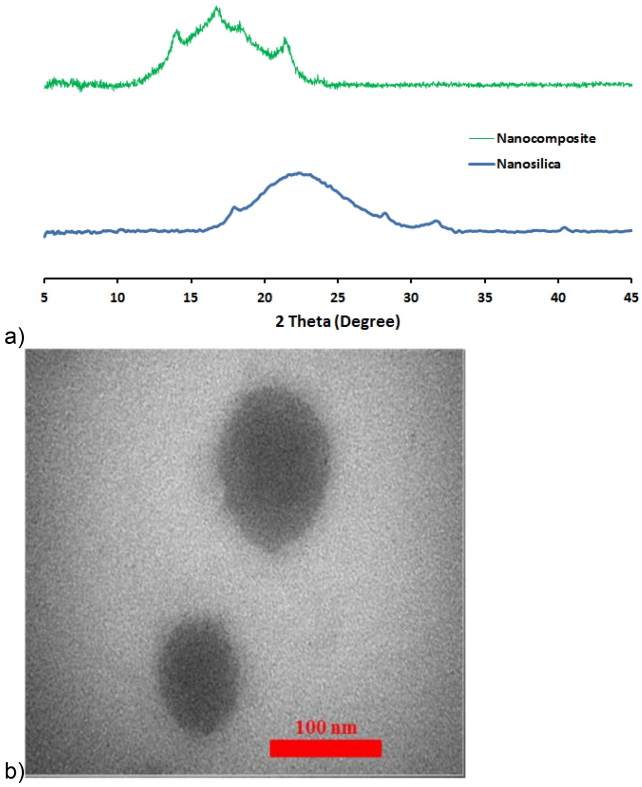

Figure 8. (a) XRD patterns of neat nanocilica and HDPE/silica nanocomposite and (b) TEM image of HDPE/silica nanocomposite.

Conclusions

Here, we aim to reveal the effect of chain microstructure on the ESCR characteristic of HDPE. To this end, 5 commercial HDPE samples with various densities but similar molar mass and MFI were assessed for mechanical and ESCR characteristics. The SSA analysis confirmed various SCB/1000 C contents of the studied samples. After the mechanical and ESCR analysis data, the HDPE microstructure in terms of SCB/1000 C has a significant effect on the ESCR characteristic. As a consequence, it is advised that HDPE density should be set at its lowest extent in industrial plants in order to get the maximum ESC resistance. In addition, we next wanted to enhance the polymer ESCR by taking advantage of the nanocomposite strategy. According to the results, by incorporating 3 wt.

The percentage of modified nano-silica into the HDPE matrix, the ESCR characteristic can be significantly improved, up to 40%. These achievements help polyethylene producers to offer highly improved HDPE fabrics towards ESCR characteristics. The involvement of the comonomer was revealed through complementary DFT calculations, which provided quantitative information through the analyses of the radical dissociation of fragments of the polymer chains and qualitative insights through NCI plots since the additional ethyl chains enhance the non-innocent weak interactions between chains.

Experimental Details

Materials

The studied HDPE samples were blow molding type, BL3 grade, were kindly donated by Kermanshah Polymer Company. These polymers are produced over a heterogeneous $MgCl_2$(ethoxide type)/$TiCl_4$ Ziegler-Natta catalyst Table 1, using two continuous reactors operating at the reaction conditions of Table 2. Hexene, 5-hexene-1-ol, and heptane were purchased from Merck Co, Germany. Silica nanoparticles with diameter of 50 nm was acquired from Alfa (Karlsruhe, Germany).

Synthesis of $MgCl_2$(Ethoxide Type)/$TiCl_4$ Ziegler-Natta Catalyst in Industrial Plant

A bench-scale procedure for the production of employed Ziegler-Natta catalyst is provided here. A 1.0 L autoclave reactor with a steel jacket, blade mixer, dropping funnel, a high-precision syringe pump, temperature and pressure indicators, various inlet and outlets, was used as the main reactor where the synthesis takes palce. Milled magnesium ethoxide (10 g) and hexane (190 mL) were fed into the reactor under nitrogen atmosphere. The temperature was set at 0 °C, at which $TiCl_4$ (20 mL) was added dropwise (rate = 5 ml/h) using a syringe pump with continuous stirring (180 rpm). The temperature was then raised to 80 °C, at a rate of 1 °C/min. After 1 h maintaining this temperature, the reactor was decanted. Another 20 mL of $TiCl_4$ was added in one portion, after 1 h, the

© 2024 The Author(s). Chemistry - A European Journal published by Wiley-VCH GmbH

15213765, 2024, 54, Downloaded from https://chemistry-europe.onlinelibrary.wiley.com/doi/10.1002/chem.202401926 by Universitat de Girona, Wiley Online Library on [09/12/2024]. See the Terms and Conditions (https://onlinelibrary.wiley.com/terms-and-conditions) on Wiley Online Library for rules of use; OA articles are governed by the applicable Creative Commons License

15213765, 2024, 54, Downloaded from https://chemistry-europe.onlinelibrary.wiley.com/doi/10.1002/chem.202401926 by Universitat de Girona, Wiley Online Library on [09/12/2024]. See the Terms and Conditions (https://onlinelibrary.wiley.com/terms-and-conditions) on Wiley Online Library for rules of use; OA articles are governed by the applicable Creative Commons License

reactor was decanted and the catalyst was washed with hexane four times. The final catalyst was stored in a hexane medium.

Synthesis of Copoly(hexane/hexanol)

A 2506 mL stainless steel pressurized reactor was used to perform cooligomerization experiment. The reactor was purged with N_2 gas at 806 °C for 30 min, to remove air and possible water contamination. The temperature was cooled down to 40 °C and fed with $AlCl_3$ (0.7 g), 1-hexene (15 mL), 5-hexene-1-ol (7 mL) and ethanol (0.01 mL). After 2 h stirring, the product was evacuated and washed three times with NaOH/H_2O solution (5 wt.%). Eventually, unreacted monomers were removed by vacuum distillation at 200 °C and −0.8 mbar.

Grafting of Copoly(hexane/hexanol) onto the Nanosilica

The nanosilica particles were calcined at 550 °C for 6 h to remove absorbed water and some OH groups on the surface. 6 g of calcined silica was dispersed in dry heptane using ultrasonic irradiation in a round bottom flask for 15 min. 4 g of the synthesized copoly(hexane/hexanol) and 0.01 g potassium carbonate were added to the flask under N_2 atmosphere. The temperature was raised to 100 °C and the reaction continued for 24 h with stirring. Subsequently, the mixture was centrifuged to separate the powder, rinsed with heptane to remove unreacted copolymer and solvent. Finally, the product was dried in a vacuum oven at 80 °C, for 12 h.

Characterization

The studied HDPEs and the commercial Ziegler-Natta catalyst were analyzed using different techniques and tools such as X-ray diffraction (XRD), Brunauer–Emmett–Teller (BET), laser particle size analyzer (LPS), scanning electron microscope (SEM), Fourier-transform infrared spectroscopy (FTIR), melt flow index (MFI), Gel Permeation Chromatography (GPC), successive self-nucleation and annealing (SSA),[68] notched impact, tensile and ESCR tests. Specification of each instrument and test conditions are provided below.

XRD of the catalyst was recorded using STOE-IPDS 2T diffractometer utilizing graphite monochromatic Cu–Ka as electrode. BET examinations using a BELSORP Mini II instrument were conducted to determine specific surface area of the catalyst. The catalyst particle size was measured using LPS (the Malvern Zetasizer Nano ZS instrument, United Kingdom) according to ISO 13320–2 standard. The morphology of the employed Ziegler-Natta catalyst was observed using an SEM-EDAX coupled instrument (SEM model S-3000 N, Hitachi, Japan). The comonomer content was measured via FTIR spectroscopy (Bruker Tensor 27 spectrometer), using Montell test method, MTM 15984E. The procedure is based on ASTM D 2238–68 standard test method which considers the absorption band of the CH_3 segment at 769 and 1378 cm^{-1}.[69] The MFI characteristic of the polymers was measured employing an Extrusion Plastometer of the Italian producer ATS Faar S.p.a. company using 5.0 and 21.6 kg weights, following the procedure mentioned in ASTM D1238 and ISO 1133, *i.e.* at T = 190 °C. The impact test of the samples was carried out in a Zwick 4 impact machine (Germany), according to ASTM D-256 procedure. For the mentioned test, three notched specimens for each sample were prepared using a circular profile blade with 1 mm radius. The temperature, humidity and displacement rate were T = 23 °C, 50% RH and 10 mm/min, respectively, during test experiments.

The chain structure of the polymers was evaluated using SSA analysis employing DSC Mettler Toledo (Switzerland) instrument, under N_2 atmosphere. SSA fractionation was performed using a procedure reported by some of us.[1] The Lamellar thickness and comonomer percentage were calculated using T_m of distinct melting peaks appearing in the SSA thermograms using the formulae indicated in references.[70] High temperature GPC analysis was conducted utilizing a Viscotek system (from Malvern Instruments, Agilent Technologies) equipped with three columns and a refractive index type detector. To perform this test, 1,2,4-trichlorobenzene was eluant that stabilized with BHT (butylated hydroxytoluene, with the concentration of 200 mg/L). The flow rate and temperature were 1 mL/min of 150 °C, respectively. Furthermore, 200 μL solution of each polymer sample with a concentration of 5 mg/mL was injected into each test.

The tensile properties of the studied HDPEs were recorded using a Zwick tensile tester (ZwickRoell group, Germany) at room temperature according to the ASTM d638 standard. To prepare the samples for the tensile test, the specimens (at least three for each sample) were compression molded into a 1 mm thick dumb-bell shape. The test conditions were T = 23 °C, displacement rate = 10 mm/min and humidity 50% RH. In the tensile test, the applied force and the resulting elongation were measured simultaneously at regular intervals and the results are plotted in the form of stress–strain curves, see Figure S4. These tests were repeated three times for each sample, and the average values are reported here with an accuracy of ±5%.

The ESCR characteristics of the samples were assessed using the iPT ESCR tester instrument (Germany) following the instruction of the ASTM D 1693 (2)2015 standard. The chemical reagent was nonylphenoxy poly(ethyleneoxy)ethanol. For ESCR measurements, notched U shape specimens with 39×9×13 mm dimension were placed in a nonylphenoxy poly(ethyleneoxy)ethanol solution at T = 50 °C. The test was continued until a 50% failure occurs.

Computational Details

Density functional theory (DFT) calculations were performed with the Gaussian16 package.[71] Geometry optimizations were performed via the spin-restricted Kohn-Sham (RKS) formalism with the M062X functional of Truhlar,[72] together with the split valence basis set (Def2-SVP keyword in Gaussian),[73] including the D3 version of Grimme's dispersion (empiricaldispersion = GD3).[74] Frequency calculations were performed to confirm the nature of the stationary points. Single point energy calculations were performed employing the M062X–D3 functional together with the Def2-TZVP basis set.[75]

Supporting Information Summary

Additional supporting information can be found online in the Supporting Information section at the end of this article.

Acknowledgements

N.B.-L. is thankful to Iran National Science Foundation for financial support of the work under the grant number of 4006310. C.Z is thankful to National Natural Science Foundation of China under the grant number of 22261142664. The authors would like to thank Iran Polymer and Petrochemical Institute (IPPI) and Kermanshah Polymer Company for partial support of this work. A.P. thanks the ICREA Academia Prize 2019. We thank the Spanish Ministerio de Ciencia e Innovación for project

© 2024 The Author(s). Chemistry - A European Journal published by Wiley-VCH GmbH

PID2021-127423NB–I00 and the Generalitat de Catalunya for project 2021SGR623. A.P. is a Serra Húnter Fellow. Open Access funding provided thanks to the CRUE-CSIC agreement with Wiley.

Conflict of Interests

The authors declare no conflict of interest.

Data Availability Statement

The data that support the findings of this study are available from the corresponding author upon reasonable request.

Keywords: High density polyethylene · Environmental Stress Cracking Resistance (ESCR) · Ziegler-Natta catalyst · Short chain branch · Lamella thickness

[1] a) M. Stürzel, S. Mihan, R. Mülhaupt, *Chem. Rev.* **2016**, *116*, 1398–1433; b) A. Tennakoon, X. Wu, A. L. Paterson, S. Patnaik, Y. Pei, A. M. LaPointe, S. C. Ammal, R. A. Hackler, A. Heyden, I. I. Slowing, G. W. Coates, M. Delferro, B. Peters, W. Huang, A. D. Sadow, F. A. Perras, *Nat. Catal.* **2020**, *3*, 893–901.
[2] A. Shams, M. Mehdizadeh, H. R. Teimoury, M. Emami, S. A. Mirmohammadi, S. Sadjadi, E. Bardají, A. Poater, N. Bahri-Laleh, *J. Ind. Eng. Chem.* **2022**, *116*, 359–370.
[3] a) S. Sánchez-Valdes, *Iran. Polym. J.* **2021**, *30*, 297–305; b) R. Cong, A. Parrott, C. Hollis, M. Cheatham, T. Hill, K. Bailey, Z. Zhou, J. Bautista, P. Balding, J. Fan, *Macromolecules* **2023**, *56*, 1492–1502; c) T. B. Mikenas, E. I. Koshevoy, S. V. Cherepanova, V. A. Zakharov, *J. Polym. Sci., Part A: Polym. Chem.* **2016**, *54*, 2545–2558.
[4] a) Y. V. Kissin, T. E. Nowlin, R. I. Mink, *Handbook of Transition Metal Polymerization Catalysts* **2018**, 189–227; b) S. H. Kang, H. M. Lee, K. W. Kim, B. J. Byung, *J. Ind. Eng. Chem.* **2023**, *19*, 1722–1729; c) A. Ribas-Massonis, M. Cicujano, J. Duran, E. Besalú, A. Poater, *Polymers* **2022**, *14*, 2856; d) M. M. Hassan, R. O. Aly, S. E. Abdel Aal, A. M. El-Masry, E. S. Fathy, *J. Ind. Eng. Chem.* **2015**, *19*, 1722–1729.
[5] Y. J. Yim, S. J. Park, *J. Ind. Eng. Chem.* **2015**, *21*, 155–157.
[6] B. H. Choi, J. Weinhold, D. Reuschle, M. Kapur, *Polym. Eng. Sci.* **2009**, *49*, 2085–2091.
[7] a) I. Kuryndin, S. Kostromin, R. Mamalimov, A. Chervov, A. Grebennikov, S. Bronnikov, *Polyolefins J.* **2022**, *9*, 25–31; b) Y. Chen, *J. Appl. Polym. Sci.* **2014**, *131*, 39880; c) A. Almomani, A. H. I. Mourad, S. Deveci, J. W. Wee, B. H. Choi, *Mater. Des.* **2023**, *227*, 111720; d) M. H. Jandaghian, A. Sepahi, S. Hosseini, R. Esmaeilzade, E. Nikzinat, M. Masoori, K. Afzali, *J. Appl. Polym. Sci.* **2024**, *141*, e55078; e) M. H. Jandaghian, Y. Maddah, A. Sepahi, S. Houshmandmoayed, E. Nikzinat, M. Masoori, K. Afzali, R. Rashedi, *J. Appl. Polym. Sci.* **2022**, *139*, 51867; f) J. W. Wee, A. Chudnovsky, B. H. Choi, *Int. J. Mech. Sci.* **2023**, *257*, 108546; g) H. Bazgir, A. Sepahi, Sh. Hosseini, K. Afzali, S. Houshmandmoayed, E. Nikzinat, R. Rashedi, *J. Polym. Res.* **2023**, *30*, 58.
[8] A. Gobetti, G. Ramorino, *J. Polym. Res.* **2020**, *27*, 353.
[9] a) S. Ki Ng, M. A. Kamaludin, J. P. Dear, B. R. Blackman, *Procedia Struct. Integr.* **2018**, *13*, 304–310; b) M. Contino, L. Andena, M. Rink, G. Marra, *Eng. Fract. Mech.* **2018**, *203*, 32–43; c) L. Andena, M. Rink, C. Marano, F. Briatico-Vangosa, L. Castellani, *Polym. Test.* **2016**, *54*, 40–47.
[10] a) M. Contino, L. Andena, M. Rink, *Eng. Fract. Mech.* **2021**, *241*, 107422; b) M. A. Kamaludin, Y. Patel, J. G. Williams, B. R. K. Blackman, *Theor. Appl. Fract. Mech.* **2017**, *92*, 373–380; c) M. A. Kamaludin, Y. Patel, B. R. K. Blackman, J. G. Williams, *Procedia Struct. Integr.* **2016**, *2*, 227–234.
[11] a) M. Contino, L. Andena, V. La Valle, M. Rink, G. Marra, S. Resta, *Mech. Time Depend. Mater.* **2020**, *24*, 381–394; b) M. Contino, L. Andena, M. Rink, A. Colombo, G. Marra, *Procedia Struct. Integr.* **2016**, *2*, 213–220.
[12] L. Andena, L. Castellani, A. Castiglioni, A. Mendogni, M. Rink, F. Saccheti, *Eng. Fract. Mech.* **2013**, *101*, 33–46.
[13] a) L. Trávníček, J. Poduška, J. Kučera, L. Náhlík, P. Hutař, *Procedia Struct. Integr.* **2023**, *43*, 148–153; b) A. Sharif, N. Mohammadi, S. R. Ghaffarian, *J. Appl. Polym. Sci.* **2009**, *112*, 3249–3256.
[14] a) Y. F. Men, J. Rieger, H. F. Enderle, D. Lilge, *Eur. Phys. J. E* **2004**, *15*, 421–425; b) Y. Tang, Z. Jiang, Y. Men, L. An, H. F. Enderle, D. Lilge, S. V. Roth, R. Gehrke, J. Rieger, *Polymer* **2007**, *48*, 5125–5132.
[15] M. J. Shirkavand, H. Azizi, I. Ghasemi, M. Karabi, *Adv. Polym. Technol.* **2018**, *37*, 21719.
[16] A. Moyassari, T. Gkourmpis, M. S. Hedenqvist, U. W. Gedde, *Macromolecules* **2019**, *52*, 807–818.
[17] J. J. Strebel, *Polym. Test.* **1995**, *14*, 189–202.
[18] M. Thuy, M. Pedragosa-Rincón, U. Niebergall, H. Oehler, I. Alig, M. Böhning, *Polymers* **2022**, *14*, 2415.
[19] X. Guo, L. Cui, J. Yi, Z. Liu, B. Liu, *J. Phys. Chem. C* **2022**, *126*, 8655–8666.
[20] T. Wada, G. Takasao, A. Piovano, M. D'Amore, A. Thakur, P. Chammingkwan, P. C. Bruzzese, M. Terano, B. Civalleri, S. Bordiga, E. Groppo, T. Taniike, *J. Catal.* **2020**, *385*, 76–86.
[21] A. Piovano, M. Signorile, L. Braglia, P. Torelli, A. Martini, T. Wada, G. Takasao, T. Taniike, E. Groppo, *ACS Catal.* **2021**, *11*, 9949–9961.
[22] K. S. Thushara, M. D'Amore, A. Piovano, S. Bordiga, E. Groppo, *ChemCatChem* **2017**, *9*, 1782–1787.
[23] T. B. Mikenas, V. A. Zakharov, M. A. Matsko, *Iran. Polym. J.* **2022**, *31*, 471–484.
[24] R. Bazvand, N. Bahri-Laleh, M. Nekoomanesh, H. Abedini, *Des. Monomers Polym.* **2015**, *18*, 599–610.
[25] A. Piovano, E. Groppo, *Coord. Chem. Rev.* **2022**, *451*, 214258.
[26] a) C. Cattò, F. Secundo, G. James, F. Villa, F. Cappitelli, *Int. J. Mol. Sci.* **2018**, *19*, 4003; b) P. Ding, X. Zheng, L. Ma, *Polym. Test.* **2023**, *122*, 108027; c) A. Almomani, S. Deveci, A. H. I. Mourad, I. Barsoum, *Polym. Test.* **2023**, *118*, 107911.
[27] Reviews in predictive chemistry a) R. Monreal-Corona, A. Pla-Quintana, A. Poater, *Trends Chem.* **2023**, *5*, 935–946; b) S. Escayola, N. Bahri-Laleh, A. Poater, *Chem. Soc. Rev.* **2024**, *53*, 853–882.
[28] Examples of predictive chemistry a) R. Monreal-Corona, À. Díaz-Jiménez, A. Roglans, A. Poater, A. Pla-Quintana, *Adv. Synth. Catal.* **2023**, *365*, 760–766; b) M. Gimferrer, N. Joly, S. Escayola, E. Viñas, S. Gaillard, M. Solà, J. L. Renaud, P. Salvador, A. Poater, *Organometallics* **2022**, *41*, 1204–1215; c) N. Joly, M. Gimferrer, S. Escayola, M. Cendra, S. Coufourier, J. F. Lohier, Q. Gaignard Gaillard, S. Gaillard, M. Solà, J. L. Renaud, A. Poater, *Organometallics* **2023**, *42*, 1784–1792; d) R. Monreal-Corona, E. Besalú, A. Pla-Quintana, A. Poater, *Org. Chem. Front.* **2022**, *9*, 4347–4357; e) M. Tomasini, J. Zhang, H. Zhao, E. Besalú, L. Falivene, L. Caporaso, M. Szostak, A. Poater, *Chem. Commun.* **2022**, *58*, 9950–9953.
[29] M. H. Jandaghian, Y. Maddah, E. Nikzinat, M. Masoori, A. Sepahi, R. Rashedi, S. Houshmandmoayed, R. Davand, K. Afzali, *J. Macromol. Sci., Part A* **2021**, *58*, 492–498.
[30] a) S. Sadjadi, N. Abedian-Dehaghani, M. M. Heravi, X. Zhong, P. Yuan, J. Duran, A. Poater, N. Bahri-Laleh, *J. Mol. Liq.* **2023**, *382*, 121847; b) A. Rezaeian, A. Hanifpour, H. R. Teimoury, M. Nekoomanesh-Haghighi, M. Ahmadi, N. Bahri-Laleh, *Polym. Bull.* **2023**, *80*, 1625–1639.
[31] N. Ghasemi Hamedani, H. Arabi, F. Poorsank, *New J. Chem.* **2020**, *44*, 15758–15768.
[32] N. Bahri-Laleh, A. Hanifpour, S. A. Mirmohammadi, A. Poater, M. Nekoomanesh-Haghighi, G. Talarico, L. Cavallo, *Prog. Polym. Sci.* **2018**, *84*, 89–114.
[33] D. M. Stelescu, A. Airinei, M. Homocianu, N. Fifere, D. Timpu, M. Aflori, *Polym. Test.* **2013**, *32*, 187–196.
[34] H. J. Kim, J. J. Lee, J. C. Kim, Y. C. Kim, *J. Ind. Eng. Chem.* **2010**, *16*, 406–410.
[35] K. S. Thushara, E. S. Gnanakumar, R. Mathew, R. K. Jha, T. G. Ajithkumar, P. R. Rajamohanan, K. Sarma, S. Padmanabhan, S. Bhaduri, C. S. Gopinath, *J. Phys. Chem. C* **2011**, *115*, 1952–1960.
[36] F. Nouri-Ahangarani, N. Bahri-Laleh, M. Nekoomanesh-Haghighi, M. Karbalaie, *Des Monomers Polym.* **2016**, *19*, 394–405.
[37] M. Fallah, N. Bahri-Laleh, K. Didehban, A. Poater, *Appl. Organomet. Chem.* **2020**, *34*, e5333.
[38] L. Mandelkern, Crystallization of Polymers, 2nd ed.; Cambridge University Press: Cambridge, Vol. 2, 2004.
[39] C. Stern, A. Frick, G. Weickert, *J. Appl. Polym. Sci.* **2007**, *103*, 519–533.
[40] H. Zhou, G. L. Wilkes, *Polymer* **1997**, *38*, 5735–5747.
[41] A. Shahin, I. Barsoum, M. D. Islam, *Polym. Test.* **2020**, *91*, 106800.
[42] S. Y. Lee, J. Y. Jho, W. Huh, *J. Ind. Eng. Chem.* **1998**, *3*, 258–262.
[43] A. M. Mansouri, M. Emami, S. Yousefi, C. Chen, M. H. Gargari, A. Hanifpour, N. Bahri-Laleh, *J. Appl. Polym. Sci.* **2022**, *139*, e52877.

© 2024 The Author(s). Chemistry - A European Journal published by Wiley-VCH GmbH

15213765, 2024, 54, Downloaded from https://chemistry-europe.onlinelibrary.wiley.com/doi/10.1002/chem.202401926 by Universitat de Girona, Wiley Online Library on [09/12/2024]. See the Terms and Conditions (https://onlinelibrary.wiley.com/terms-and-conditions) on Wiley Online Library for rules of use; OA articles are governed by the applicable Creative Commons License

[44] a) J. D. Hoffman, R. L. Miller, *Macromolecules* **1992**, *25*, 2221–2229; b) J. D. Hoffman, R. L. Miller, *Polymer* **1997**, *38*, 3151–3212.
[45] A. G. Simanke, G. B. Galland, R. Baumhardt Neto, R. Quijada, R. S. Mauler, *J. Appl. Polym. Sci.* **1999**, *74*, 1194–1200.
[46] R. S. Ruminten, B. A. Herlambang, *Macromol. Symp.* **2020**, *391*, 1900191.
[47] a) A. Masoud Pourrahimi, L. K. H. Pallon, D. Liu, T. Anh Hoang, S. Gubanski, M. S. Hedenqvist, R. T. Olsson, U. W. Gedde, *ACS Appl. Mater. Interfaces* **2016**, *8*, 14824–14835; b) M. Zhao, H. Chen, Z. Zhu, X. Zhu, Y. Quan, Z. Zhang, H. M. Wu, J. L. Wu, W. H. Kang, Q. Wang, H. J. Sue, *Polymer* **2022**, *261*, 125422; c) M. Zare, M. Ehsani, A. Abbas, S. Akmal, R. Khajavi, D. Zaarei, *Polym.-Plast. Tech. Mat.* **2023**, *63*, 399–418.
[48] J. B. P. Soares, R. F. Abbott, J. D. Kim, *J. Polym. Sci. B: Polym. Phys.* **2000**, *38*, 1267–1275.
[49] C. De Rosa, O. Ruiz de Ballesteros, R. Di Girolamo, A. Malafronte, F. Auriemma, G. Talarico, M. Scoti, *Polym. Chem.* **2020**, *11*, 34–38.
[50] F. Jani, A. Sepahi, S. K. Afzali, S. Houshmand Moayed, *Polym. Eng. Sci.* **2023**, *63*, 176–188.
[51] J. Poater, M. Gimferrer, A. Poater, *Inorg. Chem.* **2018**, *57*, 6981–6990.
[52] M. Tabrizi, S. Sadjadi, G. Pareras, M. Nekoomanesh-Haghighi, N. Bahri-Laleh, A. Poater, *J. Colloid Interface Sci.* **2021**, *581*, 939–953.
[53] E. R. Johnson, S. Keinan, P. Mori-Sanchez, J. Contreras-Garcia, A. J. Cohen, W. T. Yang, *J. Am. Chem. Soc.* **2010**, *132*, 6498–6506.
[54] J. Contreras-Garcia, E. R. Johnson, S. Keinan, R. Chaudret, J. P. Piquemal, D. N. Beratan, W. T. Yang, *J. Chem. Theory Comput.* **2011**, *7*, 625–632.
[55] C. J. Richmond, S. Escayola, A. Poater, *Eur. J. Inorg. Chem.* **2019**, *2019*, 2101–2108.
[56] J. Masdemont, J. A. Luque-Urrutia, M. Gimferrer, D. Milstein, A. Poater, *ACS Catal.* **2019**, *9*, 1662–1669.
[57] S. Dehghani, S. Sadjadi, N. Bahri-Laleh, M. Nekoomanesh-Haghighi, A. Poater, *Appl. Organomet. Chem.* **2019**, *33*, e4891.
[58] A. Brotons-Rufes, N. Bahri-Laleh, A. Poater, *Faraday Discuss.* **2023**, *244*, 252–268.
[59] R. A. Boto, J. Contreras-Garcia, J. Tierny, J. P. Piquemal, *Mol. Phys.* **2015**, *114*, 1406–1414.
[60] a) M. Ahmadi, F. Panahi, N. Bahri-Laleh, M. Sabzi, G. Pareras, B. N. Falcone, A. Poater, *Chem. Mater.* **2022**, *13*, 6155–6169; b) M. Ahmadi, L. Löser, G. Pareras, A. Poater, K. Saalwächter, S. Seiffert, *Chem. Mater.* **2023**, *35*, 4026–4037.
[61] a) M. Kim, K. Hyun, *Rheol. J.* **2021**, *33*, 25–36; b) E. S. Trofimchuk, I. B. Meshkov, M. N. Kandlina, N. I. Nikonorova, A. M. Muzafarov, I. A. Malyshkina, M. A. Moskvina, F. I. Grabovenko, A. L. Volynskii, *Macromol. Mater. Eng.* **2019**, *304*, 1900430; c) E. Laguna-Gutierrez, C. Saiz-Arroyo, J. I. Velasco, M. A. Rodriguez-Perez, *Eur. Polym. J.* **2016**, *81*, 173–185.
[62] A. Hanifpour, N. Bahri-Laleh, S. A. Mirmohammadi, *Polym. Compos.* **2019**, *40*, 1053–1060.
[63] A. Rahbar, B. Falcone, G. Pareras, M. Nekoomanesh-Haghighi, N. Bahri-Laleh, A. Poater, *ChemPlusChem* **2023**, *88*, e202200432.
[64] W. Zhang, A. A. Dehghani-Sanij, R. S. Blackburn, *Prog. Nat. Sci.* **2018**, *18*, 801–805.
[65] L. Lin, A. K. Schlarb, *J. Mater. Sci.* **2012**, *47*, 6614–6620.
[66] H. Zhang, Z. Zhang, J. L. Yang, K. Friedrich, *Polymer* **2006**, *47*, 679–689.
[67] J. Yu, G. Wang, J. Chen, X. Zeng, W. Wang, *Polym. Eng. Sci.* **2007**, *47*, 201–206.
[68] L. Sangroniz, B. Wang, Y. Su G Liu, D. Cavallo, D. Wang, A. J. Müller, *Prog. Polym. Sci.* **2021**, *115*, 101376.
[69] J. Ruokolainen, R. Mezzenga, G. H. Fredrickson, E. J. Kramer, P. D. Hustad, G. W. Coates, *Macromolecules* **2005**, *38*, 851–860.
[70] a) M. Masoori, M. Nekoomanesh, S. Posada-Pérez, R. Rashedi, N. Bahri-Laleh, *Polymer* **2022**, *261*, 125423; b) M. Ahmadi, S. M. M. Mortazavi, S. Ahmadjo, M. Zahmati, K. Valieghbal, D. Jafarifar, R. Rashedi, *Polyolefins J.* **2016**, *3*, 135–146; c) J. Lou, K. Zhang, S. Qim, Y. Lei, Y. Liu, M. He, J. Yu, *J. Ind. Eng. Chem.* **2022**, *113*, 431–438.
[71] M. J. Frisch, G. W. Trucks, H. B. Schlegel, G. E. Scuseria, M. A. Robb, J. R. Cheeseman, G. Scalmani, V. Barone, B. Mennucci, G. A. Petersson, H. Nakatsuji, M. Caricato, X. Li, H. P. Hratchian, A. F. Izmaylov, J. Bloino, G. Zheng, J. L. Sonnenberg, M. Hada, M. Ehara, K. Toyota, R. Fukuda, J. Hasegawa, M. Ishida, T. Nakajima, Y. Honda, O. Kitao, H. Nakai, T. Vreven, J. A. Montgomery, J. E. Peralta, F. Ogliaro, M. Bearpark, J. J. Heyd, E. Brothers, K. N. Kudin, V. N. Staroverov, R. Kobayashi, J. Normand, K. Raghavachari, A. Rendell, J. C. Burant, S. S. Iyengar, J. Tomasi, M. Cossi, N. Rega, J. M. Millam, M. Klene, J. E. Knox, J. B. Cross, V. Bakken, C. Adamo, J. Jaramillo, R. Gomperts, R. E. Stratmann, O. Yazyev, A. J. Austin, R. Cammi, C. Pomelli, J. W. Ochterski, R. L. Martin, K. Morokuma, V. G. Zakrzewski, G. A. Voth, P. Salvador, J. J. Dannenberg, S. Dapprich, A. D. Daniels, Ö. Farkas, J. B. Foresman, J. V. Ortiz, J. Cioslowski, D. J. Fox, Gaussian 16, Gaussian Inc., Wallingford CT, 2016.
[72] a) Y. Zhao, D. G. Truhlar, *Theor. Chem. Acc.* **2007**, *120*, 215–241; b) Y. Zhao, D. G. Truhlar, *J. Chem. Phys.* **2006**, *125*, 194101.
[73] a) F. Weigend, R. Ahlrichs, *Phys. Chem. Chem. Phys.* **2005**, *7*, 3297–3305; b) F. Weigend, *Phys. Chem. Chem. Phys.* **2006**, *8*, 1057–1065.
[74] S. Grimme, J. Antony, S. Ehrlich, H. Krieg, *J. Chem. Phys.* **2010**, *132*, 154104.
[75] T. H. Dunning Jr, *J. Chem. Phys.* **1989**, *90*, 1007–1023.

Manuscript received: May 17, 2024
Accepted manuscript online: July 17, 2024
Version of record online: September 12, 2024

© 2024 The Author(s). Chemistry - A European Journal published by Wiley-VCH GmbH

15213765, 2024, 54, Downloaded from https://chemistry-europe.onlinelibrary.wiley.com/doi/10.1002/chem.202401926 by Universitat de Girona, Wiley Online Library on [09/12/2024]. See the Terms and Conditions (https://onlinelibrary.wiley.com/terms-and-conditions) on Wiley Online Library for rules of use; OA articles are governed by the applicable Creative Commons License